Peer-reviewed version available at Coatings 2017, 7, 235; doi:10.3390/coatings7120235

*Article*

# Effect of the addition of molybdenum on the structure and corrosion resistance of zinc–iron plating

**Daichi Kosugi [1], Takeshi Hagio [1,2], Yuki Kamimoto [2] and Ryoichi Ichino [1-3,*]**

[1] Department of Chemical Systems Engineering, Graduate School of Engineering, Nagoya University, Furo-cho, Chikusa-ku, Nagoya 464-8603, Japan
[2] Green Mobility Research Institute, Institutes of Innovation for Future Society, Nagoya University, Furo-cho, Chikusa-ku, Nagoya 464-8603, Japan
[3] Institute of Materials and Systems for Sustainability, Nagoya University, Furo-cho, Chikusa-ku, Nagoya 464-8603, Japan
* Correspondence: ichino.ryoichi@material.nagoya-u.ac.jp; Tel.: +81-789-3352

**Abstract:** Zn–Ni plating is indispensable in various industries because of its high corrosion resistance. However, Ni has been reported to trigger allergies; thus, an alternative Ni-free plating is desired. Zn–Fe plating is considered to be a promising candidate, albeit its corrosion resistance still needs to be improved. The corrosion resistance of Zn–Fe plating is expected to increase by the addition of Mo as the third alloying element as it is more noble than Zn and Fe. In this study, Zn–Fe–Mo plating with a corrosion resistance nearly equivalent to that of the Zn–Ni plating was fabricated. Zn–Fe–Mo plating was electrically deposited from continuously agitated plating baths prepared by mixing $ZnSO_4$, $FeSO_4$, $Na_2MoO_4$, $Na_3C_6H_5O_7$, and $Na_2SO_4$ using Fe or Ni plates as the substrate. The surface morphology, composition, crystal phase, and electronic state of Mo of the platings were investigated by SEM-EDS, XRD, and XPS. The anti-corrosion performance was evaluated by Tafel extrapolation method. Formation of plating comprising a Mo containing alloy phase was found to be crucial for improving corrosion resistance. The Zn–Fe–Mo plating demonstrates promise for replacing anti-corrosion Zn–Ni platings.

**Keywords:** Zn–Ni plating; Zn–Fe plating; anti-corrosion performance; Mo addition; alloy formation

## 1. Introduction

Metals such as steel and cast iron are typically used as the major components of architecture and machines in daily life [1]. In several cases, these metals are exposed to harsh environments, and protection against corrosion is a critical issue particularly where high reliability is required. The application of corrosion-resistant alloys, including stainless steels, is an effective solution; however, the high cost hinders its applications for daily use [2]. Another promising method to improve corrosion resistance is protection by Zn plating or so-called galvanization [3]. It protects the underlying steel or cast iron by the sacrificial corrosion protection effect, and its considerably lower cost has led to its widespread use in various fields.

Currently, protection coatings with a high corrosion resistance are desired to extend the life of industrial products for realizing a sustainable society and for withstanding a more severe environment to meet industrial demands. Alloying with iron-group elements such as Fe and Ni is well known in improving the corrosion resistance of Zn platings [4–8]. By the formation of alloys of Zn with iron-group elements, the standard electrode potential of the alloy becomes closer to that of the substrate metal. The smaller potential difference between the plating and substrate decreases the driving force for the corrosion of the plating, which, in turn, improves its corrosion resistance. In particular, Zn–Ni plating has demonstrated to exhibit five to six times greater corrosion resistance compared with that of Zn plating according to salt spray tests [8]. Thus, Zn–Ni plating has become

Peer-reviewed version available at Coatings 2017, 7, 235; doi:10.3390/coatings7120235



indispensable for various applications, including aircraft and automotive parts, where conventional Zn plating cannot be applied [9].

Meanwhile, in recent years, Ni allergies have become a social concern. In fact, allergic contact dermatitis in children is caused by nickel [10]. Nickel ions released from various alloys are potent allergens or haptens that can trigger skin inflammation [11]. Therefore, an alternative nontoxic Ni-free plating with a corrosion resistance equivalent to or higher than that of Zn–Ni plating is desired. Zn–Fe plating is considered to be promising because of its cost-effectiveness and nontoxicity. However, it exhibits insufficient corrosion resistance, corresponding to only one-third of that of the Zn–Ni plating [12]. Meanwhile, the addition of noble elements such as Mo and W into plating has been reported to improve the corrosion resistance via the stabilization of the passive film [13,14]. Mo and W cannot be electrically deposited from solutions alone, but these elements have been reported to undergo co-deposition with iron-group elements [15,16]. This result indicated that these elements are also possibly co-deposited into Zn–Fe platings; however, studies of Zn–Fe–Mo plating have been rarely reported thus far to the best of our knowledge [17–21]. In this study, Zn–Fe–Mo plating was electrically deposited by the addition of Mo into the plating bath, and its effect on corrosion resistance was investigated. Furthermore, the possibility of using Zn–Fe–Mo platings to replace conventional Zn–Ni platings was discussed.

## 2. Materials and Methods

### *2.1. Bath preparation*

Table 1 shows the composition of the bath, which was prepared by mixing zinc sulfate heptahydrate ($ZnSO_4 \cdot 7H_2O$, Nacalai Tesque, Inc.), iron(II)sulfate heptahydrate ($FeSO_4 \cdot 7H_2O$, Nacalai Tesque, Inc.), sodium molybdate dihydrate ($Na_2MoO_4 \cdot 2H_2O$, Kishida Chemical Co., Ltd.), trisodium citrate dihydrate ($C_6H_5Na_3O_7 \cdot 2H_2O$, Nacalai Tesque, Inc.), and sodium sulfate ($Na_2SO_4$, Nacalai Tesque, Inc.). Typically, 60 mL of distilled water (DI) was first added into a 100-mL Pyrex glass beaker, and $C_6H_5Na_3O_7 \cdot 2H_2O$, $Na_2SO_4$, $Na_2MoO_4 \cdot 2H_2O$, $ZnSO_4 \cdot 7H_2O$, and $FeSO_4 \cdot 7H_2O$ were added in the order mentioned. Second, the pH was adjusted using sodium hydroxide (NaOH, Nacalai Tesque, Inc.) and sulfuric acid ($H_2SO_4$, Nacalai Tesque, Inc.) solutions, respectively, and the total bath volume was adjusted to 100 mL by the addition of distilled water. All procedures were carried out under continuous agitation. Finally, oxygen was removed from the bath by bubbling with Ar for 30 min before use.

**Table 1.** Bath compositions used in this study

| Type of bath | Composition of bath (mol $dm^{-3}$) | | | | |
|---|---|---|---|---|---|
| | $ZnSO_4$ | $FeSO_4$ | $Na_2MoO_4$ | $C_6H_5Na_3O_7$ | $Na_2SO_4$ |
| Base | - | - | - | 0.2 | 0.1 |
| Zn | 0.2 | - | - | 0.2 | 0.1 |
| Fe | - | 0.2 | - | 0.2 | 0.1 |
| Zn-Fe | 0.2 | 0.2 | - | 0.2 | 0.1 |
| Zn-Fe-Mo | 0.2 | 0.2 | 0.01-0.1 | 0.2 | 0.1 |

### *2.2. Preparation of Zn–Fe–Mo platings by electrodeposition*

All electrochemical experiments were carried out using a three-electrode system. The electrodeposition of the Zn–Fe–Mo alloy was carried out at a fixed amount of electricity of 50 C using the bath prepared in Section 2.1. The plating bath was stirred at a constant speed of 300 rpm

Peer-reviewed version available at Coatings 2017, 7, 235; doi:10.3390/coatings7120235



using a magnetic stirrer at room temperature (25 °C). A potential/galvanostat (HZ-7000, Hokuto Denko Co.) was utilized to control the electrolysis potential and analyze data. A Ni plate (NI-313374, Nilaco) or an Fe plate (B-60-P01, Yamamoto-Ms) and a Pt coil were used as the cathode and anode, respectively. Ag/AgCl in saturated KCl was used as the reference electrode. The cathode was degreased with ethanol, pickled with 10% $H_2SO_4$, and masked with an insulation tape (PES-01, AS ONE), leaving a space of 400 $mm^2$ (20 mm × 20 mm) for electrodeposition prior to the experiment.

### *2.3. Characterization and evaluation of the platings*

Scanning electron microscopy (SEM; JSM-6330F, JEOL) equipped with energy-dispersive spectroscopy (EDS; JED2140-GS, JEOL) was employed to examine the surface morphology and composition of the plating. X-ray diffraction (XRD, Ultima IV, Rigaku) was employed to examine the crystalline phase. X-ray photoelectron spectroscopy (XPS, ESCA-3300, Shimadzu Corporation) was employed to examine the electronic state of Mo. Ar etching was performed for 3 min to confirm the electronic state of Mo inside the plating. Current efficiency ($C_{eff}$) was calculated from the mass change and plating composition, as shown in (1).

$$C_{\mathrm{eff}} = \frac{Z_{\mathrm{Zn}} n_{\mathrm{Zn}} F + Z_{\mathrm{Fe}} n_{\mathrm{Fe}} F + Z_{\mathrm{Mo}} n_{\mathrm{Mo}} F}{Q}. \quad (1)$$

Here, $Z_X$ ($X$ = Zn, Fe, or Mo) is the ionic valence of each element, $n_X$ is the molar amount obtained from EDS analysis, F is the Faraday constant, and $Q$ is the amount of electricity passed.

The corrosion resistance was evaluated by anode polarization tests. A 3 mass% sodium chloride (NaCl, Nacalai Tesque, Inc.) solution degassed with Ar was used as the test solution, with a sweep rate of 1 $mVs^{-1}$ for the polarization measurement. The potential at 0.1 $mAcm^{-1}$ in the anode polarization curve was defined as the corrosion potential ($E_{corr}$). Zn, Zn–Fe, and Zn–Ni plating were prepared and evaluated as a reference.

## 3. Results and Discussions

### *3.1. Effect of bath pH on Zn–Fe–Mo platings*

Zn–Fe–Mo plating was electrically deposited at various pH values. The current density was fixed at 10 $mAcm^{-2}$. A black precipitate with low adhesion was formed on the substrate during electrodeposition at a pH greater than 5.7. Thus, the pH range was selected from 4.0 to 5.7. Figure 1 shows the SEM images of the platings deposited in the baths at different pH values. The surface morphology clearly changed. The plating obtained from the bath at pH 4 comprised granules of c.a. 2 µm (Figure 1(a)), whereas that obtained from pH 4.5 to 5.5 changed to a fibrous structure (Figure 1(b–d)). Finally, that from pH 5.7 exhibited a smooth structure comprising fine grains (Figure 1(e)).

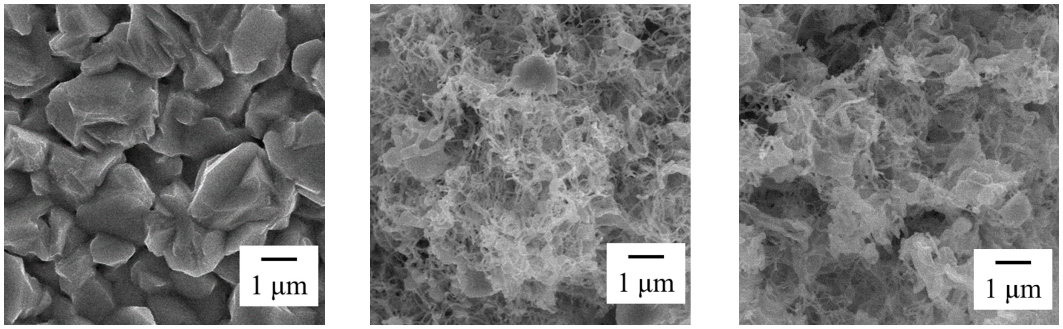


(**a**) (**b**) (**c**)

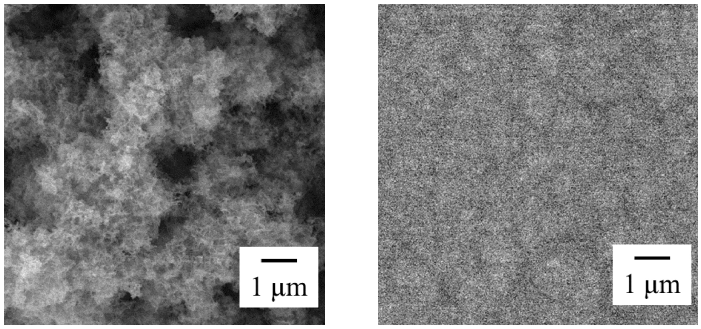


(**d**) (**e**)

**Figure 1.** SEM images of the Zn–Fe–Mo platings deposited at various pH values. (a) pH 4.0, (b) pH 4.5, (c) pH 5.0, (d) pH 5.5, and (e) pH 5.7

Figure 2 shows the composition of the platings deposited at various pH values. Ni substrates were used in this experiment to avoid the detection of Fe from the substrate. A majority of the platings exhibited a high Zn content, with only trace Fe and Mo, indicating that the current conditions are categorized as "anomalous codeposition" [22]. Although Mo was barely observed for the plating prepared by electrical deposition at pH between 4.0 and 5.2, the amount of Mo increased with further increasing pH. Moreover, at a pH of 5.7, the plating exhibited 3 at% Mo, probably related to the difference in the present form of Mo. In solution, Mo exists as oxyanions, which is known to form various polyoxyanion at low pH and mono-oxyanions at pH greater than around 6. Therefore, the deposition of Mo is thought to occur with the decrease in the size of oxyanions, which allows for the easier deposition of Mo [23,24].

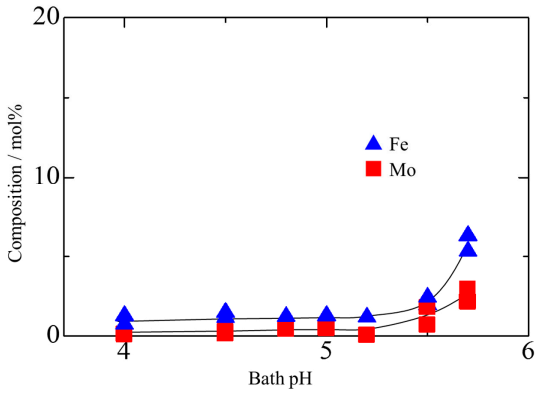


**Figure 2.** Content of Fe and Mo in Zn–Fe–Mo plating deposited at various pH values

Figure 3 shows the XRD patterns of the platings deposited at various pH values. Intense peaks were observed for all platings, indicative of the deposition of a crystalline structure. Reflections only corresponding to the Zn phase and the substrate were observed in the platings deposited at pH 4.0–5.5; however, with increasing pH, a slight shift toward low angles was observed, in addition to peak broadening. The incorporation of Fe atoms into the Zn lattice was anticipated to lead to a distorted Zn structure. Peaks other than Zn were observed for the plating obtained at pH 5.7. These are expected to correspond to reflections from a $Fe_3Mo$ based alloy phase since similar peaks have been observed for $Fe_3Mo$ alloys in previous studies [25,26].

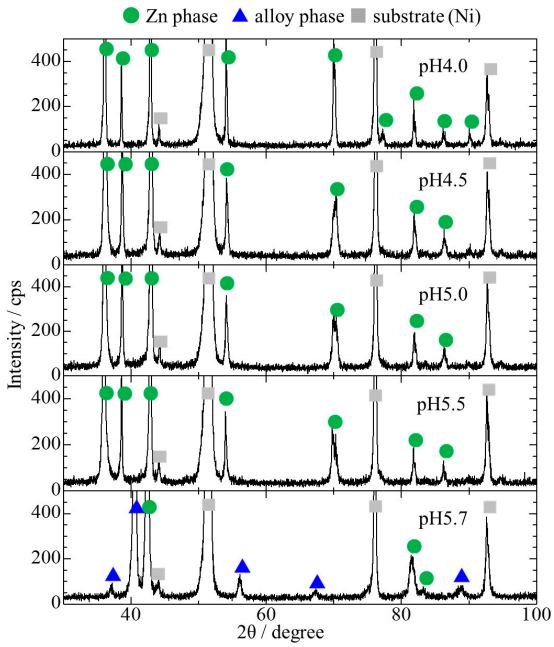


**Figure 3.** XRD patterns of the Zn–Fe–Mo plating deposited at various pH values

Figure 4 shows the anodic polarization curves of platings deposited at various pH values. The plating deposited at pH 4.0 exhibited a sharp increase in current density at around −960 mV, whereas that deposited at pH values of 4.5 exhibited a slight increase at around −1100 mV and a drastic increase at around −960 mV. At pH 5.0 and 5.5, a gradual increase between −1100 mV to −920 mV and a similar behavior to that at pH 4.0 was observed with a sharp change at around -990 mV, respectively. This indicated a low corrosion potential for the fibrous structure. For the platings deposited at pH 5.7, a change at −950 mV and a drastic change at −700 mV were observed. The plating with the supposed $Fe_3Mo$ based alloy phase exhibited higher corrosion resistance than those of the others comprising the Zn phase. From these experiments, a pH of 5.7 is selected for the remaining experiments.

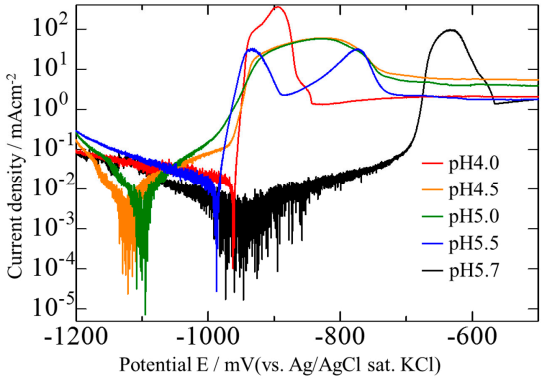


**Figure 4.** Anodic polarization curves of the Zn–Fe–Mo plating deposited at various pH values

*3.2. Effect of current density on Zn–Fe–Mo platings*

A cathodic polarization measurement was carried out to consider the range of current density. Figure 5 shows the measured cathodic polarization curves at a pH of 5.7 and a sweep rate of 5 mV/s. The deposition of Zn and Fe started at approximately −1080 and −980 mV from baths containing Zn

Peer-reviewed version available at Coatings 2017, 7, 235; doi:10.3390/coatings7120235



or Fe alone (Zn and Fe baths), respectively. Meanwhile, when using the plating bath containing both Zn and Fe (Zn–Fe bath), a small peak at −980 mV and a second large peak were observed at −1080 mV, corresponding to the deposition of Fe and Zn, respectively. Finally, from the bath containing Zn, Fe, and Mo, two peaks were again observed at −800 mV, possibly corresponding to the co-reduction of Fe and Mo, and at −1200 mV, related to Zn deposition. These shifts in potential are likely to be explained by the presence of noble Mo, shifting the reduction of Fe to higher potentials through co-reduction of Mo while shifting the Zn deposition to lower potential by avoiding the deposition of Zn via the adsorption of oxyanions on substrate surface.

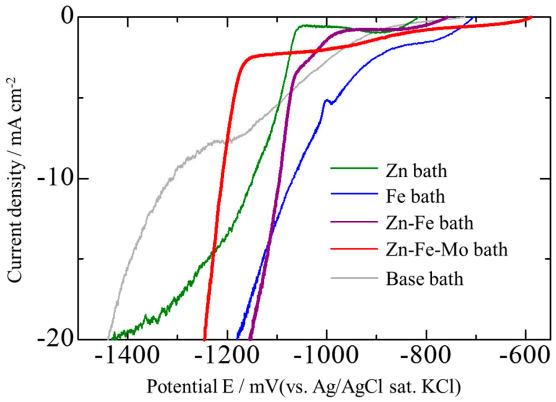


**Figure 5.** Cathodic polarization curves obtained from different baths

From the results obtained from the cathodic polarization curves, current densities of 1, 2, 5, and 10 $mAcm^{-2}$ were selected. Figure 6 shows the SEM images of the platings deposited at different current densities. At low current densities, the plating surface comprised bulky granules (Figure 6(a)). The size decreased with increasing current density, probably because a high current density promoted the nucleation on the substrate surface.

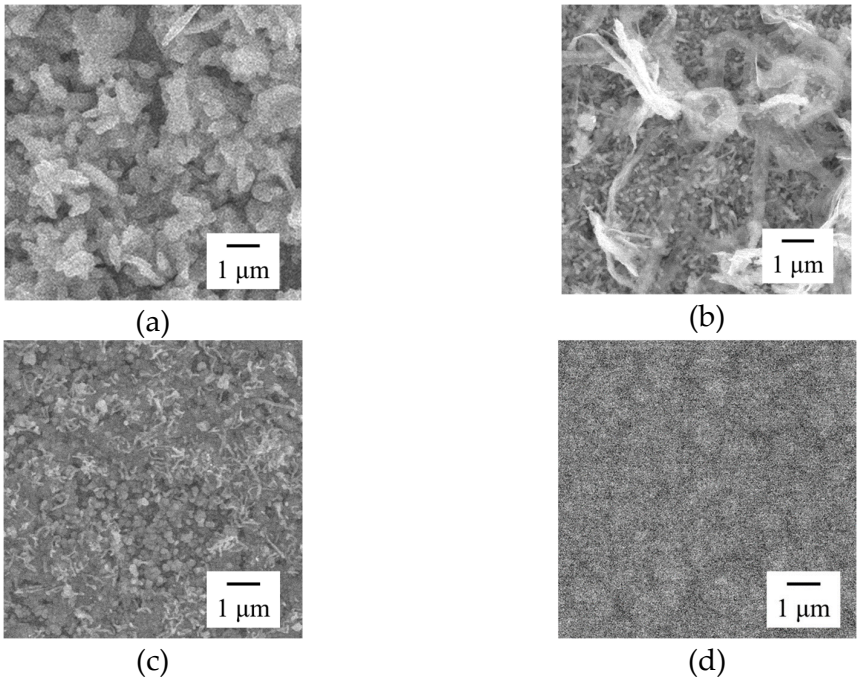


**Figure 6.** SEM images of the Zn–Fe–Mo plating deposited at various current densities (a) 1 $mAcm^{-2}$, (b) 2 $mAcm^{-2}$, (c) 5 $mAcm^{-2}$, and (d) 10 $mAcm^{-2}$

Figure 7 shows the relationship between the plating composition and current density. The content of Mo in the plating decreased with increasing current density, possibly corresponding to a high deposition rate of the plating and an insufficient feed rate of the Mo ions. The extremely high deposition rate must have led to the depleted Mo layer near the substrate surface, thereby leading to the slow reduction of Mo [27].

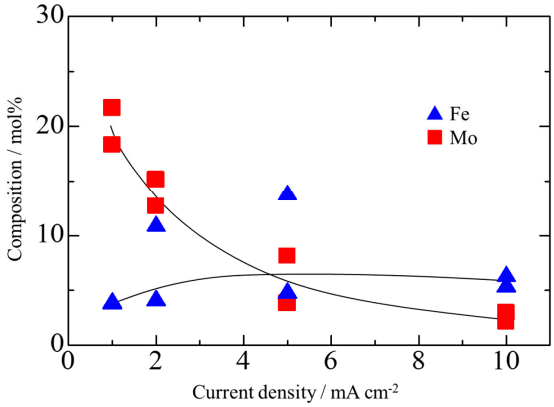


**Figure 7.** Content of Fe and Mo in the Zn–Fe–Mo plating deposited at various current densities

Figure 8 shows the result obtained from the XPS analysis of platings deposited at different current densities. The peaks around 227 to 228 eV corresponds to metal Mo (Mo (0)) and 229 to 234 eV corresponds to Mo in the oxide or hydroxide state. Mo (0) was not observed on the plating surface. For the platings deposited at 1 and 2 mAcm$^{-2}$, changes were not observed even after Ar-ion etching; however, Mo (0) was observed for plating at 5 and 10 mA/cm$^2$ after Ar-ion etching, indicating that a relatively high current density is required to reduce Mo, which is necessary for co-deposition to occur. The low generation rate of atomic hydrogen at the substrate surface may be responsible for this phenomenon since Mo is proposed to be reduced by the generation of atomic hydrogen in previous studies [27,28]. Similar results have been reported for electroplating in a Ni–Mo system [27].

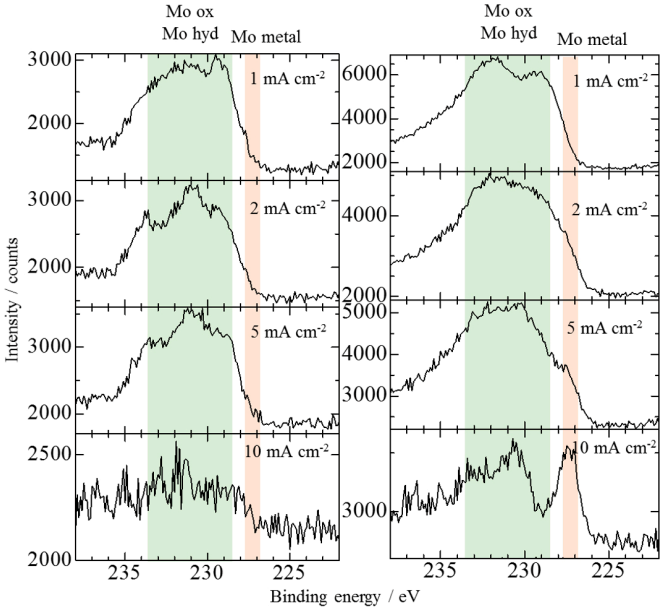


**Figure 8.** XPS analysis results of the Zn–Fe–Mo platings deposited at various current densities

Figure 9 shows the relationship between the current density and current efficiency. The current efficiency increased with current density. As the amount of electricity was constant, a low current density is equivalent to a long electrodeposition time. The decrease in the current efficiency at low current density is assumed to be related to the dissolution of oxygen from the atmosphere into the plating bath, leading to necessity of extra electricity to reduce the dissolved oxygen in the bath.

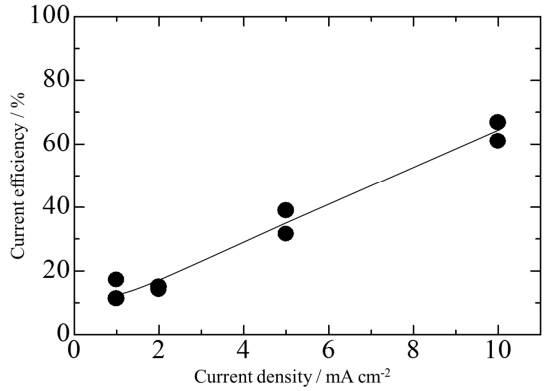


**Figure 9.** Relationship between current density and current efficiency

Figure 10 shows the XRD patterns of the platings deposited at various current densities. With increasing current density, peaks corresponding to the alloy phase were observed. The peak of the alloy phase became more intense as the current density increased. Even though a large amount of Mo was detected in platings deposited at low current densities, Mo could not be reduced to form alloys and could only exist as oxides or hydroxides.

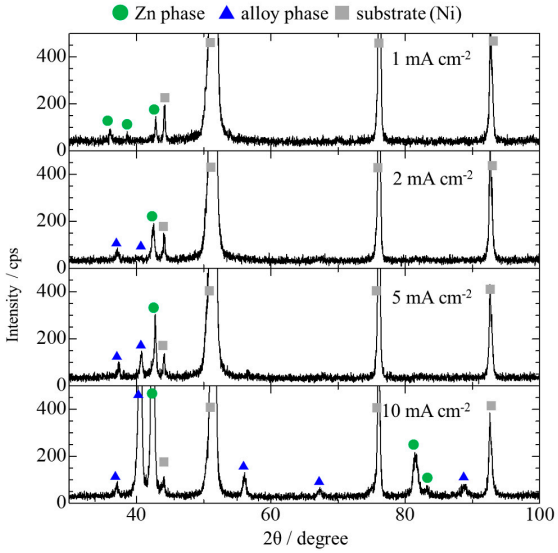


**Figure 10.** XRD patterns of the Zn–Fe–Mo platings deposited at various current densities

Figure 11 shows the anodic polarization curves of platings deposited at various current densities. With increasing current density, the potential shifted to a more noble value. The presence of an alloy phase is indicated to be crucial as anticipated in Section 3.1.

Peer-reviewed version available at Coatings 2017, 7, 235; doi:10.3390/coatings7120235



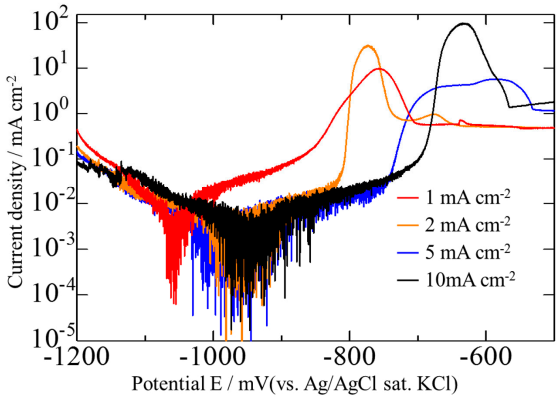


**Figure 11.** Anodic polarization curves of the Zn–Fe–Mo platings deposited at various current densities

*3.3. Effect of Mo concentration of plating bath on Zn-Fe-Mo platings*

The SEM image of platings obtained when using plating baths with different Mo concentration is shown in Figure 12. The Mo concentration was 0.01, 0.02 and 0.1 moldm$^{-3}$. The plating obtained from the 0.01 moldm$^{-3}$ Mo containing bath showed smooth and homogeneous surface; however, small cracks were observed by increasing the Mo concentration to 0.02 moldm$^{-3}$ and a rough surface with even more cracks were observed by further increasing the Mo concentration to 0.1 moldm$^{-3}$. An increase in Mo concentration of the plating bath seems to have negative effect on plating quality.

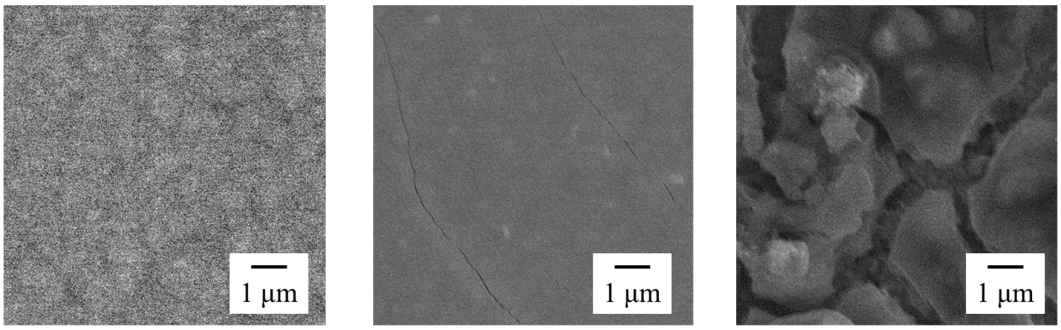


**Figure 12.** SEM image of Zn-Fe-Mo plating deposited at various Mo concentration (a) 0.01 mol dm$^{-3}$ (b) 0.02 mol dm$^{-3}$ (c) 0.1 mol dm$^{-3}$

The composition of Mo content in the platings are shown in Figure 13. An increase in the content of Fe and Mo in the platings was observed by increasing the Mo concentration of the plating bath. This is because more $MoO^{2-}$ were supplied and adsorbed onto the surface of the substrate along with the increase in Mo concentration in the plating bath.

Peer-reviewed version available at Coatings 2017, 7, 235; doi:10.3390/coatings7120235



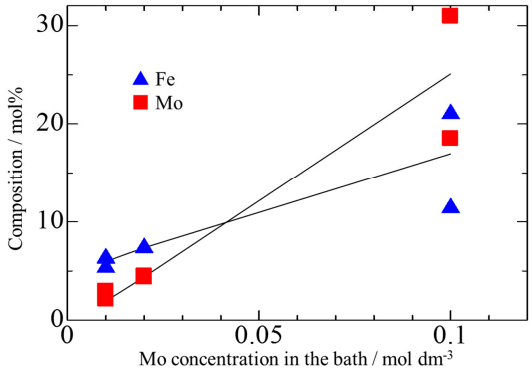


**Figure 13.** Content of Fe and Mo in the Zn–Fe–Mo plating deposited from a plating bath with different Mo concentration

Figure 14 shows the result obtained from the XPS analysis of platings deposited from plating baths with different Mo concentrations. Again, Mo (0) was not observed on the plating surface. After Ar-ion etching, Mo (0) was observed for plating deposited from baths containing 0.01 and 0.02 moldm$^{-3}$ Mo; however, not from baths containing 0.1 moldm$^{-3}$ Mo. At low Mo concentration, both Fe and hydroxide of Mo by reduction of $MoO^{2-}$ shall coexist on the surface of the substrate and Mo may be thus reduced since the atomic hydrogen can be held at the unpaired 3d electrons on the Fe metals [28]. In contrast, at high Mo concentrations, the surface of the substrate will be covered with excess hydroxides of Mo, making it difficult for Fe to approach the plating surface. Thus, further reduction of hydroxides of Mo must be prevented due to the lack of Fe; i.e., the lack of atomic hydrogen. Zn must have been prevented as well by the hydroxide of Mo.

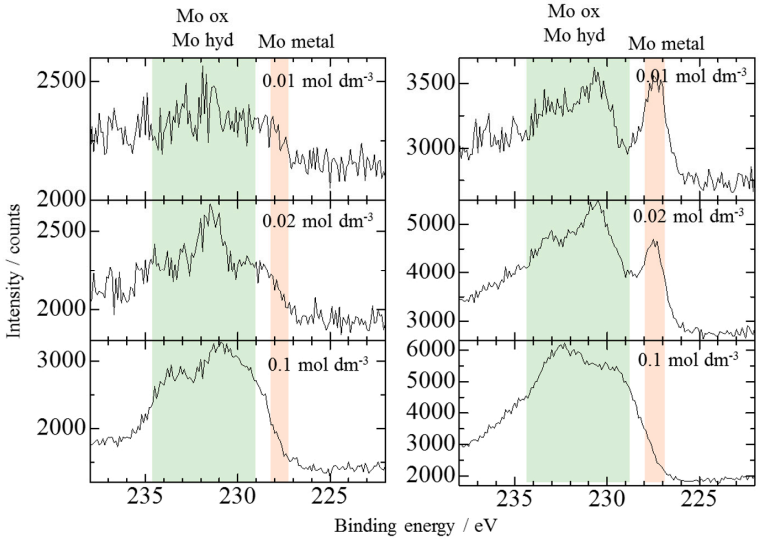


**Figure 14.** XPS analysis results of the Zn–Fe–Mo plating deposited from a plating bath with different Mo concentration

Figure 15 shows the relationship between the Mo concentration in the plating bath and current efficiency. The current efficiency decreased by increasing the Mo concentration in the plating bath. The increasing formation of hydroxide of Mo on the surface prevents Fe deposition, resulting in a lower current efficiency [29]. The trend of current efficiency seems to support this expectation.

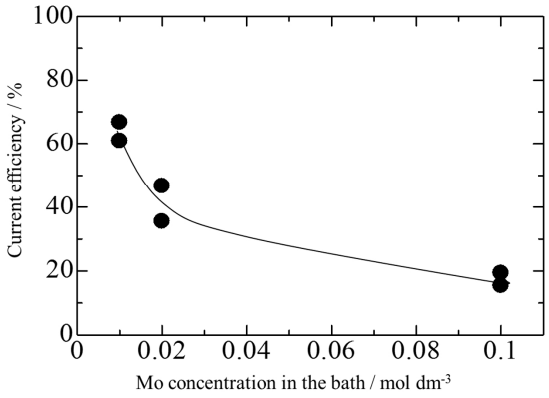


**Figure 15.** Relationship between Mo concentration and current efficiency

Figure 16 shows the XRD patterns of the platings deposited from baths of various Mo concentrations. The intense peaks of alloy phase were detected as decreasing the Mo concentration. This also supports the idea that Mo in the plating existed in the Mo (0) form and lower Mo concentration led to enhanced formation of Mo (0).

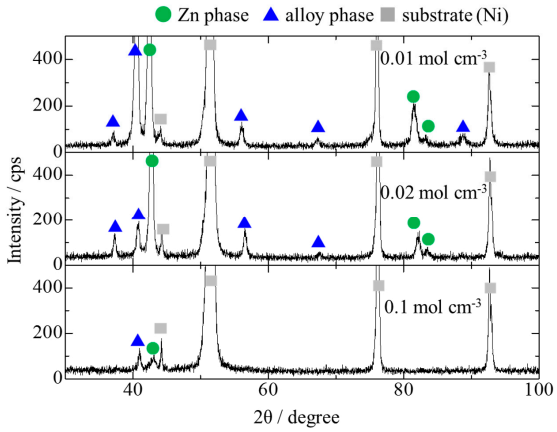


**Figure 16.** XRD patterns of the Zn–Fe–Mo plating deposited from a plating bath with different Mo concentration

Figure 17 shows the anodic polarization curves of platings deposited from baths with various Mo concentrations. All three platings showed relatively noble potentials. A decrease in Mo concentration of the plating bath, corresponding to more intense peaks of alloy phase, shifted the potential to a more noble value. Again, the results support the idea that presence of alloy phase is importance.

Preprints (www.preprints.org) | NOT PEER-REVIEWED | Posted: 24 November 2017 doi:10.20944/preprints201711.0162.v1

Peer-reviewed version available at Coatings 2017, 7, 235; doi:10.3390/coatings7120235



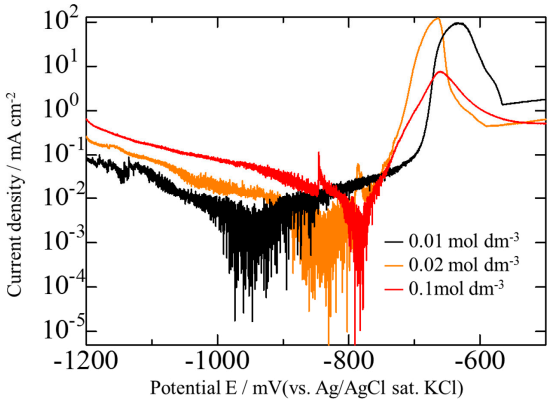


**Figure 17.** Anodic polarization curves of the Zn–Fe–Mo platings deposited at various Mo concentration

### *3.4. Corrosion potentials of the Zn–Fe–Mo platings*

Figure 18 shows the relationship between the content of Mo in the plating and $E_{corr}$, as well as the $E_{corr}$ values for Zn, Zn–Fe, and Zn–Ni plating. A low Mo content led to high $E_{corr}$; however, it was not proportional to the content of Mo in the plating. This indicated that the Mo content in the plating is not the primary factor improving the corrosion resistance of the plating.

Figure 19 shows the relationship between the peak intensity ratio of the alloy and Zn phases from XRD and $E_{corr}$ to discuss the effect of alloy phase. Peaks corresponding to the alloy and Zn phases were observed at 2θ values of 40.7° and 42.8°, respectively, apparently indicating that the deposition of the alloy phase is crucial for high corrosion resistance.

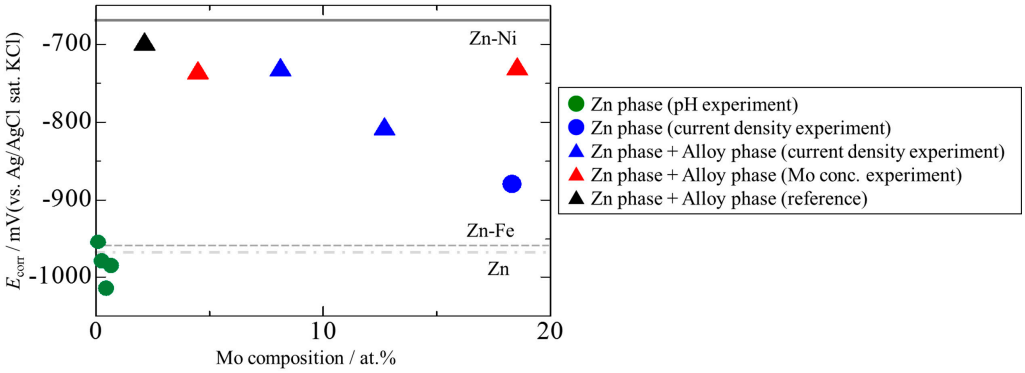


**Figure 18.** Relationship between the content of Mo in the plating and $E_{corr}$

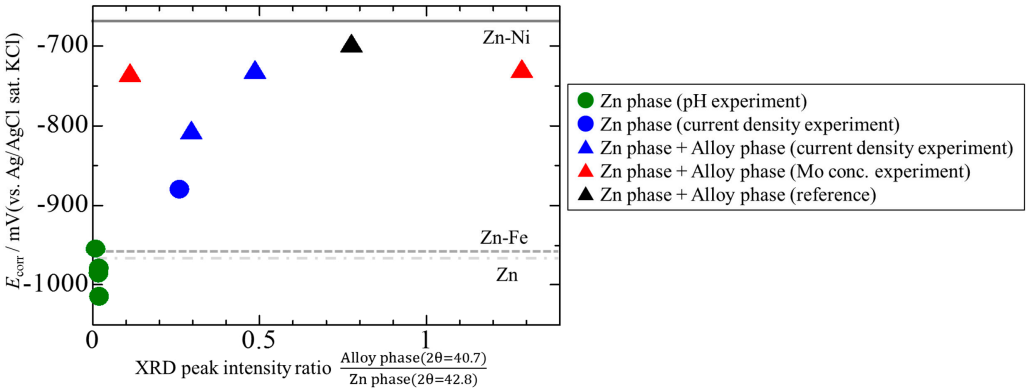


**Figure 19.** Relationship between the peak intensity ratio of the alloy phase and Zn phase from the XRD and $E_{corr}$

## 4. Conclusions

In this study, the addition of Mo into the Zn–Fe platings was considered to improve its corrosion resistance. The following results were obtained.

1. The Zn–Fe–Mo platings obtained by this experiment exhibited high corrosion resistance when the electrically deposited layer formed a $Fe_3Mo$ based alloy phase.
2. The best plating exhibited high corrosion resistance comparable with that of Zn–Ni platings, revealing promise for Zn–Fe–Mo platings as potential alternatives for Zn–Ni platings.
3. For the co-deposition of Mo, it is crucial to control the pH to approximately 5.7 to ensure that Mo does not form large polyoxides and Zn does not form hydroxides.
4. Co-deposition does not effectively occur at low current densities, and a high Mo concentration in the bath as Mo (IV) cannot be efficiently reduced to Mo (0).

**Author Contributions:** D. Kosugi mainly performed the experiments and analyses; T. Hagio considered the data and wrote the paper; Y. Kamimoto gave important advice throughout the experiments; and R. Ichino conceived and designed the experiments.

**Conflicts of Interest:** The authors declare no conflict of interest.

## References


1. Nesic, S.; Postlethwaite, J.; Olsen, S. An electrochemical model for prediction of corrosion of mild steel in aqueous carbon dioxide solutions. *Corrosion* **1996**, *52*, 280-294, DOI: 10.5006/1.3293640.
2. Lo, K.H.; Shek, C.H.; Lai, J.K.L. Recent developments in stainless steels. *Mater. Sci. Eng.* **2009**, *65*, 39–104, DOI: 10.1016/j.mser.2009.03.001.
3. Mackowiak, J.; Short, N.R. Metallurgy of galvanized coatings. *Int. Met. Rev*, **1979**, *24*, 1-19, DOI: 10.1179/imtr.1979.24.1.1
4. Byk, T.V.; Gaevskaya, T.V.; Tsybulskaya, L.S. Effect of electrodeposition conditions on the composition, microstructure, and corrosion resistance of Zn–Ni alloy coatings. *Surf. Coat. Technol.* **2008**, *202*, 5817–5823, DOI: 10.1016/j.surfcoat.2008.05.058.
5. Tozar, A.; Karahan, I.H. Structural and corrosion protection properties of electrochemically deposited nano-sized Zn–Ni alloy coatings. *Appl. Surf. Sci.* **2014**, *318*, 15–23, DOI: 10.1016/j.apsusc.2013.12.020.
6. Yadav, A.P.; Katayama, H.; Noda, K.; Masuda, H.; Nishikata, A.; Tsuru, T. Effect of Fe-Zn alloy layer on the corrosion resistance of galvanized steel in chloride containing environments. *Corros. Sci.* **2007**, *49*, 3716–3731, DOI: 10.1016/j.corsci.2007.03.039.
7. Boshkov, N.; Petrov, K.; Vitkova, S.; Nemska, S.; Raichevsky, G. Composition of the corrosion products of galvanic alloys Zn–Co and their influence on the protective ability. *Surf. Coat. Technol.* **2002**, *157*, 171–178, DOI: 10.1016/S0257-8972(02)00161-5.
8. Shibuya, A.; Kurimoto, T.; Korekawa, K.; Noji, K. Corrosion-resistance of electroplated Ni-Zn alloy steel sheet. *Tetsu-to-Hagane* **1980**, *7*, 771-778, DOI: 10.2355/tetsutohagane1955.66.7_771. (Japanese)
9. Gnanamuthu, M.R.; Mohan, S.; Saravanan, G.; Leea, C.W. Comparative study on structure, corrosion and hardness of Zn–Ni alloy deposition on AISI 347 steel aircraft material. *J. Alloys Compd.* **2012**, *513*, 449-454, DOI: 10.1016/j.jallcom.2011.10.078.
10. Goldenberg, A.; Admani, S.; Janice J. L.; Jacob, S.E. Belt buckles—increasing awareness of nickel exposure in children: a case report. *PEDIATRICS* **2015,** *136*, 691-693, DOI: 10.1542/peds.2015-0794
11. Saito, M.; Arakaki, R.; Yamada, A, Tsunematsu, T.; Kudo, Y.; Ishimaru, N. Molecular mechanisms of nickel allergy. *Mol. Sci.* **2016**, *17*, DOI: 10.3390/ijms17020202 www.mdpi.com/journal/
12. Qun, Z.L. Electrodeposition of zinc-iron alloy from an alkaline zincate bath. *Met. Finish.* **1998**, *96*, 56-57, DOI: 10.1016/S0026-0576(98)80872-6.
13. Sriraman, K.R.; Raman, S.G.S.; Seshadri, S.K. Corrosion behaviour of electrodeposited nanocrystalline Ni–W and Ni–Fe–W alloys. *Mater. Sci. Eng.* **2007**, *460–461*, 39-45, DOI: 10.1016/j.msea.2007.02.055.
14. Naka, M.; Hashimoto, K.; Masumoto, T. High corrosion resistance of amorphous Fe-Mo and Fe-W alloys in HCl. *J. Non-Cryst. Solids* **1978**, *29*, 61-65, DOI: 10.1016/0022-3093(78)90140-0.
15. Akiyama. T.; Fukushima, H. Recent study on the iron-group metal alloy. *ISIJ Int.* **1992**, *32*, 787-798, DOI: 10.2355/isijinternational.32.787.
16. Podlaha. E.J.; Landolt, D. Induced codeposition I. An experimental investigation of Ni-Mo alloys. *J. Electrochem. Soc.* **1996**, *143*, 885-892, DOI: 10.1149/1.1836553.
17. Winiarski, J.; Tylus, W.; Winiarska. K.; Szczygieł, B. The influence of molybdenum on the corrosion resistance of ternary Zn–Co–Mo alloy coatings deposited from citrate–sulphate bath. *Corros. Sci.* **2015**, *91*, 330–340, DOI: 10.1016/j.corsci.2014.11.037.
18. Szczygieł, B.; Laszczyńska, A.; Tylus, W. Influence of molybdenum on properties of Zn–Ni and Zn–Co alloy coatings. *Surf. Coat. Technol.* **2010**, *204*, 1438–1444, DOI: 10.1016/j.surfcoat.2009.09.042.
19. Keyvani, A.; Yeganeh, M.; Rezaeyan, H. Electrodeposition of Zn-Co-Mo alloy on the steel substrate from citrate bath and its corrosion behavior in the chloride media. *J. Mater. Eng. Perform.* **2017**, *26*, 1958–1966, DOI: 10.1007/s11665-017-2619-5.
20. Winiarski, J.; Tylus, W.; Krawczyk, M.S.; Szczygieł, B. The influence of molybdenum on the electrodeposition and properties of ternary Zn–Fe–Mo alloy coatings. *Electrochim. Acta* **2016**, *196*, 708–726, DOI: 10.1016/j.electacta.2016.03.027.
21. Winiarski, J.; Leśniewicz, A.; Pohl, P.; Szczygieł, B. The effect of pH of plating bath on electrodeposition and properties of protective ternary Zn–Fe–Mo alloy coatings. *Surf. Coat. Technol.* **2016**, *299*, 81–89, DOI: 10.1016/j.surfcoat.2016.04.073.
22. Gómez, E.; Pelaez, E.; Vallés, E. Electrodeposition of zinc+iron alloys: I. Analysis of the initial stages of the anomalous codeposition. *J. Electroanal. Chem.* **1999**, *469*, 139-149, DOI: 10.1016/S0022-0728(99)00196-5.

23. Gómez, E.; Pellicer, E.; Vallés, E. Influence of the bath composition and the pH on the induced cobalt–molybdenum electrodeposition. *J. Electroanal. Chem.* **2003**, *556*, 137-145, DOI: 10.1016/S0022-0728(03)00339-5.
24. Kazimierczaka, H.; Ozga, P.; Sochab, R.P. Investigation of electrochemical co-deposition of zinc and molybdenum from citrate solutions. *Electrochim. Acta* **2013**, *104*, 378–390, DOI: 10.1016/j.electacta.2012.12.140.
25. Jung, S.M. Quantitative analysis of FeMo alloys by X-Ray fluorescence spectrometry. *Am. J. Anal. Chem.* **2014**, *5*, 766-774, DOI: 10.4236/ajac.2014.512085
26. Ma, S.; Xing, J.; Fu, H. Yi, D. Zhang, J.; Li, Y.; Zhang, Z.; Zhu, B.; Ma, S. Interfacial morphology and corrosion resistance of Fe–B cast steel containing chromium and nickel in liquid zinc. *Corr. Sci.* **2011**, *53*, 2826-2834, DOI: 10.1016/j.corsci.2011.05.020
27. Chassaing, E.; Quang, K.V.; Wiart, R. Mechanism of nickel-molybdenum alloy electrodeposition in citrate electrolytes. *J. Appl. Electrochem.* **1989**, *19*, 839–844, DOI: 10.1007/BF01007931.
28. Fukushima, H.; Akiyama, T.; Akagi, S.; Higashi, K. Role of iron-group metais in the induced codeposition of molybdenum from aqueous olution. Trans. JIM 1979, 20, 358-364, DOI: 10.2320/matertrans1960.20.358
29. Kubota, A.; Tashiro, Y.; Yamasaki, K.; Nakano, H.; Oue, S.; Kobayashi, S.; Akiyama, T.; Fukushima, H. Electrodeposition behavior and properties of iron-group metal alloys with W from ammoniacal citrate baths. *Tetsu-to-Hagane* **2000**, *86*, 116-122, DOI: 10.2355/tetsutohagane1955.86.2_116. (Japanese)